SPE49447

Geological Framework Modeling and Rock Type Optimization for A Giant Oil Field, Offshore Abu Dhabi

By Sadafumi Neo, Jiro Asada, Nozomi Fujita, Salman Mohammed and Hani Arab, ZADCO, Abu Dhabi, UAE

This paper was selected for presentation at the 8th Abu Dhabi International Petroleum Exhibition and Conference held in Abu Dhabi, U A E , 11-14 October 1998
This paper was selected for presentation by the SPE Program Committee following review of information contained in an abstract submitted by the authors. Contents of the paper as presented, have not been reviewed by the Society of Petroleum Engineers and are subject to correction by authors. The material, as presented, does not necessarily reflect any position of the Society of Petroleum Engineers or its members. Papers presented at SPE meetings are subject to publication review by Editorial Committee of the Society of Petroleum Engineers. Permission to copy is restricted to an abstract of not more than 300 words. Illustration may not be copied. The abstract should contain conspicuous acknowledgment of where and by whom the paper was presented. Write Librarian, SPE, P.O.Box 8333836, Richardson, TX 75083-3836 U S A , fax 01-214-952-9435

Abstract

Reservoir characterization study was conducted to build a realistic 3D flow unit model for Thamama II carbonate reservoir by clarifying geological factors controlling highly heterogeneous permeability distribution in this reservoir.

Algal micritization was found as a key geological factor of this reservoir leading to both rock type optimization and geological framework modeling. Petrophysically, algal micritization alters grain type and pore type thoroughly by creating abundant micro-pores within grains and closing intergranular macro-pores due to easy compaction of softened grains. In terms of distribution, such algal micritization is significant mainly in a shallow shoal area according to recent carbonate analogue from offshore Abu Dhabi. A total of 10 lithofacies was defined based mainly on the composition of newly defined 8 grain types, which represent distinct micro-pore distribution, physical property and depositional environment.

Pore throat size distribution curve analysis shows that peak pore throat size from SCAL data fairly matches with calculated pore throat size using Winland equation. Petrographical and petrophysical evaluation led to fair to good poro-perm regression to a Flow Zone Indicator (FZI) curve for each lithofacies, which is reasonably explained by a unique composition of different pore types in each lithofacies. These lithofacies were further grouped into 6 rock types by FZI value.

Areal distribution of these lithofacies shows aggradational stacking pattern and abrupt lateral change particularly in Lower IIB-IID. This rather matches with detached rimmed carbonate shelf model controlled by a NW-SE trending shoal and tidal channel system, contrary to the conventional understanding of progradational carbonate ramp model for this reservoir. Two high permeability lithofacies composed of non-micritized grains and intergranular pores were recognized lying along tidal channels.

Permeability maps were preliminarily generated for key layers using lithofacies/rock type maps, unique FZI value for lithofacies/rock type and log porosity. Further optimization of rock type with relatively poor FZI regression is planned in the next phase to accomplish better match among predicted permeability, core permeability and dynamic data.

1. Introduction

A giant oil field producing oil from Lower Cretaceous Thamama I, II and III carbonate reservoirs is located offshore Abu Dhabi, extending 50 km from East to West and 30 km from North to South. Approximately 400 wells have been drilled into Thamama II reservoir by ZADCO. This reservoir has 130 - 150 feet thickness and is divided into 6 subzones, i.e., IIA to IIF in descending order.

Thamama II reservoir is highly heterogeneous in this field in terms of permeability distribution, vertically and horizontally, in spite of relatively homogeneous porosity distribution. Locally distributed thin and high permeability layers with maximum permeability up to several darcy have caused breakthrough of injected water. Test permeability map shows heterogeneous lateral permeability variation with NW-SE trending high and low permeability, although a gradual poro-perm decrease toward the structural flanks has been caused by late burial diagenesis, i.e., differential compaction and cementation. Cause of heterogeneous permeability distribution, which is independent of the structural growth, has not been geologically clarified by the previous geological studies using a conventional petrographical description technique.

The objective of this study is to clarify geological framework causing heterogeneous permeability distribution and to build a realistic 3D flow unit model based on both adequate flow unit identification and a realistic flow unit distribution along with geological framework. In order to perform this objective, two interactive work areas, i.e., rock type optimization and geological framework modeling, were set with the available data including 44 cored wells along with approximately 400 wells.

Three different types of general rock type model are shown on Fig.1. Historically, geologists constructed simple rock type models based on geological distribution information retained in lithofacies category (Fig.2). However, reservoir engineers are not satisfied by this rock type model, which has fairly large petrophysical variation in a rock type, for the reservoir simulation purpose. They require good petrophysical regression with unified pore throat size in a rock type. Accordingly, complex rock type model is built mainly based on petrophysical information (Fig.2). However distribution modeling of such rock types can not be realistic due to lack of geological distribution information. Linear interpolation method can be only applied to this rock type model. In this reservoir characterization study, rock type definition was optimized to accomplish adequate petrophysical regression in each rock type for flow unit identification and realistic rock type distribution along with geological framework for flow unit distribution.

Fig.3 shows a work flow chart of this study. In geological framework modeling area, enormous geological distribution information was extracted from the available data and a geological framework model was constructed on lithofacies basis. In rock type optimization area, the rock type scheme was established to retain geological distribution information and petrophysical information. Finally, defined rock types were incorporated into geological framework model through lithofacies and permeability mapping. Looped work flow for both rock type optimization and geological framework modeling, and also early integration of multi-disciplinary data were implemented to increase a reality of geological model. Information was always exchanged each other in the overlapping area of these two work areas.

2. Grain Type Identification

Poro-perm cross-plots in terms of matrix texture (Fig.4) and intergranular porosity occurrence (Fig.5) typically represent a complex petrographical and petrophysical relationship of reservoir rocks in this reservoir. Although some high permeability grainstones are associated with abundant intergranular pores as usual, a lot of porous grainstones and packstones/ grainstones are plotted in the lower permeability area with nil to rare intergranular pores. This means that conventional carbonate rock classification using matrix texture alone is not effective in this reservoir for the rock typing purpose.

Conventional petrographical description generally uses thin sections. However, slabbed cores were initially described in detail in this study. Fig.6 shows different grain type identification by thin section and slabbed core. Two porous grainstone samples with significant permeability difference are shown using photos of thin section and slabbed core. It is difficult to differentiate grain types between Sample 1 and Sample 2 by thin section photos (A and C) only. Grain size is not a matter in this case. In stead, slabbed core photos (B and D) show completely different grain appearance. Low permeability (9 md) of Sample 1 is explained by micro-porosity distribution only within light-colored and micritic grains and complete intergranular calcite cementation. On the other hand, high permeability (354 md) of Sample 2 is due to abundant intergranular pores preserved by dark-colored, non-micritic and hard grains. Presence of different grain types, which have formed high and low permeability rocks and can not be differentiated by thin sections, requires a step of adequate grain type identification using slabbed cores prior to lithofacies and rock type definition.

Prior to petrographical observation, surface of slabbed cores was polished using a machine for better identification of grain types. Grain type observation was initially focussed on reworked and coarse-grained intervals for easy identification. The following 8 coarse grain types were finally identified after repeated slabbed core observation of 14 key wells;

Intact and non-micritized rudist
Shell fragment
Orbitolina
Altered-bioclast
Micritic wackestone intraclast
Algal boundstone/*lithocodium* intraclast
Algal grain
Peloidal-grainstone intraclast

Fig.7 shows that this grain type identification has a key for both geological framework modeling and rock type optimization. The shallowest depositional environment is indicated at the top right corner by algal boring and encrusting, and agitation and reworking effect on grains. While process of algal boring and micritization has not been fully understood, a carbonate analogue from recent carbonate sediments reported by B.H.Purser[1] indicates a significant algal micritization in a shallow shoal area. Closely related occurrence of micritized grains to shallow lithofacies and sedimentary structures suggests syn-depositional origin of grain micritization, although microporosity formation within grains has been interpreted as late burial diagenesis for Hadriya Reservoir in Berri Field, Saudi Arabia (R.B.Koepnick et al[2]). In addition to geological distribution information in terms of depositional environment, each grain type shows different physical property and micro-porosity distribution within grain. These defined coarse grain types were successfully

applied to fine-grained intervals and the remaining 30 cored wells. After slabbed core description, thin sections were also described in terms of fine-scaled geological features such as matrix texture, cement and pore.

3. Geological Framework Modeling

After new grain type definition, enormous geological information in terms of carbonate depositional style as well as petrographical and petrophysical relationship was obtained through petrographical description of polished slabbed cores. The following interpretation in terms of geological framework of this reservoir was done based on the described reliable geological features, although some interpretations are contrary to the conventional understanding for this reservoir.

3.1 Palaeo-topography

Three reworked and coarse-grained lithofacies were defined at first based on coarse grain type composition and associated geological features (bottom schema of Fig.8). The original depositional environment of 8 grain types before reworking was estimated as shown on the top schema of Fig.8. Thin intraclast dominant coarse Packstone/(Grainstone) (LF9) is associated with erosional surface. Matrix of this lithofacies has been commonly replaced by abundant rhombic dolomites. This lithofacies has usually low permeability even in grainstones due to severe compaction of micritized and softened grains (Location A of Fig.8 & 9). On the other hand, thicker altered-bioclast dominant coarse Grainstone/Packstone (LF7) is associated with burrowed hardground surface. This lithofacies has high permeability due to preservation of intergranular pores by rigid framework of hard altered-bioclasts (Location B of Fig.8 & 9). Such observed geological features indicate that LF9 formed in a shallower depositional environment than LF7. Intermediate type of lithofacies, i.e., Mixed grain coarse Grainstone/Packstone (LF8), was also identified.

Distribution of these lithofacies indicates a clear depositional control by palaeo-topography.

3.2 Relative Sea-level Change

Three different sets of geological features were observed during slabbed core observation in three different intervals, i.e., IIE-IIF, Lower IIB-IID and IIA-Upper IIB (Fig.10). Sea-level fall, slow relative sea-level rise and high-rate relative sea-level rise were interpreted for IIE-IIF, Lower IIB-IID and IIA-Upper IIB, respectively, based on the observed different geological features. Accommodation space caused by sea-level rise was filled gradually by carbonate sediments. Consequently, generally shallow carbonate shelf environment was maintained during Thamama II depositional time, resulting in regionally correlatable blanket-type reservoir in Abu Dhabi Region.

The interpreted relative sea-level change for Thamama II reservoir was correlated to a 3rd order global eustatic cycle as shown on Fig.10. Global eustatic sea-level curve and time correlation in Ma shown by V.C.Vahrenkamp[3] were used on this figure. Rate of global eustatic sea-level change could have been modified by regional subsidence of Rub Al Khali Basin.

Thin stylolitic dense zones at the boundaries between IIA to IIF subzones are well correlated in Abu Dhabi Region. Bases of these stylolitic zones characterized commonly by erosional or burrowed surfaces were interpreted as 4th order sequence boundaries. Presence of even small amounts of clay mineral (less than 1 percent) encourages stylolite development (C.J.Burgess[4]). Abundant stylolites in these dense zones can be explained by clay mineral input during 4th order lowstand. In addition, upward fining beds with 4 to 10 feet thickness also bounded by erosional or burrowed surfaces are regarded as 5th order parasequences. Such parasequences are clearly identified with reworked lithofacies in Lower IIB-IID.

The observed vertical and lateral lithofaces variation indicates repeated and mainly aggradational deposition of lithofacies in response to 4th and 5th order relative sea-level change.

3.3 Definition and Distribution of Lithofacies

The following ten lithofacies were finally defined by grain type composition as well as matrix texture on the basis of depositional control by palaeo-topography and relative sea-level change ;

LF1 : Bioclastic Wkst/Mdst
LF2 : Peloidal Altered-bioclastic Wkst/(Pkst)
LF3 : Very Fine Peloidal Altered-bioclastic Pkst/(Grst)
LF4 : Very Fine Altered-bioclastic Peloidal Grst/Pkst
LF5 : Peloidal intraclastic foraminiferal Grst/Pkst
LF6 : Orbitolina Dominant Coarse Pkst/(Grst)/(Wkst)
LF7 : Altered-bioclast Dominant Coarse Grst/Pkst
LF8 : Mixed Grain Coarse Grainstone/Packstone
LF9 : Intraclast Dominant Coarse Pkst/(Grst)
LF10 : Dolomite

Five lithofacies from LF1 to LF5 are non-reworked and fine-grained lithofacies deposited during 5th order transgression to highstand. Rudist Floatstones frequently observed in IIA-Upper IIB are included in these fine-grained lithofacies based on the understanding that both depositional environment and petrophysical characteristics are controlled mainly by fine-grained matrix rather than scattered rudist shells. Four lithofacies from LF6 to LF9 are reworked and coarse-grained lithofacies probably formed during 5th order lowstand. LF10 is the replaced dolomite lithofacies mainly during early diagenetic phase according to fluid inclusion analysis. LF4 and LF7 have high permeability associated with intergranular pores preserved by dominant altered-bioclasts.

Stratigraphic correlation of 10 cored wells from Northwest to Southeast shows unclear lateral lithofacies change in IIE-IIF, clear lateral change and aggradational stacking of lithofacies in Lower IIB-IID and subtle progradational lithofacies stacking from NW to SE in IIA-Upper IIB (Fig.11). In addition, a weak aggradational stacking nature of lithofacies is still observed in IIA-Lower IIB. The line of this stratigraphic correlation is shown on Fig.24.

A schematic lithofacies distribution is illustrated on Fig.12 for each parasequence in these three intervals. Distinct lithofacies distribution patterns observed in these three intervals could depend on the interpreted different sea-level condition in these intervals. Reworked lithofacies mainly observed in Lower IIB-IID could have formed during 5th order lowstand under slow sea-level rising condition. Reworked LF7 with high permeability could extend in palaeo-topographic low area, where burrowed hardground surface with low permeability crust is dominantly observed at the base of this lithofacies. Vertical arrangement of these high and low permeability layeres could affect water breakthrough and vertical fluid movement in this interval. In IIA-Upper IIB, non-reworked LF4 conformably deposited under the interpreted high-rate sea-level rising condition. This high permeability LF4 could distribute at the flanks of shoals. This topographically controlled depositional style is supported by recent carbonate sand distribution around Bu Tini Shoal, offshore Abu Dhabi (B.H.Purser[1]). Peloidal foraminiferal sands with significant algal micritization observed in the lagoonal complex area of this shoal are a good analogue to low permeability LF5. Non-micritized coral/algal sands observed at the flank of this shoal are a good analogue to high permeability LF4.

Fig.13 illustrates how lithofacies stack aggradationally in Lower IIB-IID reflecting both palaeo-topography and 5th order relative sea-level change.

Major early diagenetic effect deteriorating reservoir characteristics, such as intergranular drusy calcite cementation and early compaction of micritized grains, is related to palaeo-topography in this reservoir, and has already overprinted on depositional fabric of each lithofacies. In addition, late diagenetic effect on lithofacies such as differential compaction and cementation is also incorporated into this lithofacies classification as described in Section 4.2.

3.4 Palaeo-topographic Trend

Although geological concept in terms of lithofacies distribution in this reservoir has been clarified by mainly slabbed core description, geological information in terms of dimension and trend of palaeo-topography is insufficient from only 44 cored wells out of approximately 400 wells drilled in this field. Two key geological factors to extend this geological concept to uncored wells were found during cored well evaluation. Lower IIB-IID interval in palaeo-topographic high area is thinner than that in palaeo-topographic low area due to erosion (Fig.13). In addition, rhombic dolomite tends to replace matrix of shallow lithofacies, suggesting possible meteoric water affected diagenesis. Although definite evidence of meteoric diagenesis has not been found, combined occurrence of micritized lithofacies, erosional surfaces, rhombic dolomites and abundant equant/drusy calcite cements suggests some effect of meteoric water in palaeo-topographic high area mainly during 5th order lowstand. Fig.14 shows palaeo-topographic interpretation based on porosity adjusted isopach of IID+IIE and dolomite distribution in IID and IIE. This information was derived from FDC/CNL logs of approximately 400 wells. IID+IIE interval was selected in stead of Lower IIB-IID because of easy and sure log correlation. Average porosity of IID+IIE was adjusted to 30% to recover thickness in the structural flank area where thickness had been reduced by differential compaction. Two clear trends are observed on this map. Regional thickening toward Southeast indicates a regional depositional dip at that time. NW-SE elongated palaeo-high and low areas were interpreted as a shoal and tidal channel system parallel to regional dip.

This palaeo-topographic trend map was used as a geological template for lithofacies mapping on the basis of aggradational stacking concept illustrated on Fig.13.

4. Rock Type Optimization

Petrophysical grouping using SCAL data and petrographical and petrophysical evaluation of CCAL samples on lithofacies basis were conducted prior to rock type definition. It is emphasized that lithofacies definition was optimized by an integrated and looped work of petrographical/petrophysical evaluation and geological framework modeling of lithofacies. Rock type was finally defined to satisfy both acceptable petrophysical regression in each rock type and spatially traceable rock types in line with geological framework.

4.1 Petrophysical Grouping

Petrophysical grouping was conducted at first using 277 SCAL samples. Pore throat size distribution curves converted from capillary pressure data were classified into 10 types based solely on peak pore throat size and curve shape (Fig.15). Fig.16 shows distribution of these pore throat size distribution curve types on poro-perm plot. Peak pore throat size increases notably in relation with permeability, while different curve shape types with similar peak pore throat size are plotted in the same poro-perm area. A relationship between poro-perm and peak pore throat size on Fig.16 has a good match with a relationship between poro-perm and calculated pore throat size using Winland equation shown on Fig.17, except for low porosity Type 01 and 02. This experimental equation (S.Kolodzie Jr[5]) is shown as follows;

$$\text{Log (R35)} = 0.732 + 0.588 \text{ Log (core Kh)} - 0.864 \text{ Log (core } \phi) \quad (1)$$

Where R35 : average pore throat radius(R) at 35% of pore volume filled with oil or 65% water saturation

A.J.Martin et al[6] applied this equation to carbonate reservoir rocks in Middle East, while D.Winland initially applied to sandstones. Good matching between SCAL derived peak pore throat size and calculated pore throat size using Winland equation against poro-perm indicates a possibility of pore throat size modeling and further capillary pressure modeling in this reservoir.

4.2 Petrography and Petrophysics of Lithofacies

Fig.18 shows pore throat size distribution curve plots for 10 lithofacies. Two common features are observed on these plots. (1) Each lithofacies has distinct distribution curve shape, which indicates a unique composition of several pore types in each lithofacies. This is attributed to lithofacies definition of this study, retaining distinct grain type and pore type composition as a depositional fabric overprinted by early diagenesis. (2) Variation of peak pore throat sizes is observed in each lithofacies. This can be explained by late burial diagenesis, i.e., differential compaction and cementation, based on the observation that poro-perm generally decreases toward the structural flanks in each lithofacies.

Abundant intergranular pores in very fine-grained and high permeability LF4 are represented by approximately 3-4 micron peak pore throat size. The other fine-grained lithofacies, i.e., LF1, LF2, LF3 and LF5, have mostly less than 1 micron peak pore throat size whichever matrix porosity or micro-intragranular porosity is dominant. Subordinate distribution of 3-4 micron pore throat in LF3 represents a transitional nature of this lithofacies from LF4 to LF2 in IIA-IIB. Coarse-grained and high permeability LF7 has dual porosities which larger pore throat size exceeds 10 micron.

Regression analysis of porosity and permeability was done for each lithofacies using approximately 2000 CCAL samples. Fig.19 shows an example for LF3. This lithofacies was subdivided into two sublithofacies, i.e., IIA-IIB and IIC-IIE, based on the fact that these two sublithofacies have distinct spatial distribution and petrophysical characteristics. Higher permeability distribution in IIA-IIB is attributed to more intergranular pore distribution in these subzones as a transitional facies from LF4 to LF2 (Fig.18), since high permeability LF4 mainly distributes in IIA-IIB. A good relationship is observed between poro-perm plots and a Flow Zone Indicator (FZI) curve for each of these two sublithofacies. FZI introduced by J.O. Amaefule et al[7] is defined as the following equation;

$$FZI = 1/((Fs)^{\wedge 1/2}\ \tau\ Sgv) = RQI/\phi z \quad (2)$$
$$RQI = 0.0314\ (K/\phi)^{\wedge 1/2}$$
$$\phi z = \phi/(1-\phi)$$

where : Fs : Shape factor
τ : Tortuosity
Sgv : Surface area per unit grain volume
RQI : Reservoir Quality Index

FZI is a function of tube shape and surface area per unit grain volume, which means that FZI is closely related to distributed pore type and further grain type. Therefore, poro-perm plots for each (sub)lithofacies defined based on distinct grain type and pore type composition is reasonably regressed to a FZI curve. Each FZI curve with 0.6 and 0.45 FZI values was preliminarily adopted for IIA-IIB and IIC-IIE of LF3, respectively.

Poro-perm plot for LF5 on Fig.20 shows a more scattering nature against the preliminary regression FZI curve with 0.5 FZI value. However, further subdivision of this lithofacies will be meaningless, since this scattering is mainly attributed to a micro-heterogeneity of this shallow lithofacies created by bioturbation and thin alternation.

Permeability variation in poro-perm plots for LF7 (Fig.21) is very large within moderate to high porosity range. This lithofacies was subdivided into two sublithofacies, i.e., well-sorted and poor-sorted types based on petrographical observation and an important role of the well-sorted sublithofacies in the reservoir as a breakthrough path of injected water. Although two FZI curves were applied to two sublithofacies, poro-perm scattering and limited sample number do not allow any confident regression curve particularly for the well-sorted sublithofacies. This regression analysis will be reviewed again during the planned 3D reservoir attribute modeling in the next phase. Regression FZI values for each lithofacies will be optimized by comparing modeled permeability with actual core permeability and dynamic data.

Ten lithofacies were subdivided into 13 (sub)lithofacies on the basis that sublithofacies still contain vital geological distribution information to differentiate its spatial distribution from the other (sub)lithofacies.

4.3 Rock Type Definition

Fig.22 shows schematic pore type composition for 13 (sub)lithofacies. Certain variation of pore type composition in each (sub)lithofacies reflects micro-heterogeneity within such (sub)lithofacies and lithofacies transition from one to the others, and are represented by a variation of grain volume and sorting. Frequently observed vuggy pores in this reservoir are excluded in this figure based on the scattered and separate occurrence of these pores indicating their limited contribution to poro-perm (F.J.Lucia[8]). These 13 (sub)lithofacies were finally merged into 6 rock types based on their FZI regression values as shown on Fig.22. For instance, dominant matrix porosity in mud-supported LF2 and dominant micro-intragranular

porosity in grain-supported LF5 have a similar petrophysical characteristics resulting in the same FZI regression value 0.5. Therefore, LF2 and LF5 were merged into one rock type, although such lithofacies have completely different petrographical nature. Spatial distribution of this rock type is distinct along with geological framework of lithofacies.

4.4 Permeability and Capillary Pressure Prediction

Six rock types are shown on Fig.23 by FZI curves. Iso-pore throat size curves derived from Winland equation are superimposed. This diagram suggests that this rock type concept can be applied to the prediction of permeability and capillary pressure.

Since each (sub)lithofacies is converted to one rock type and one FZI value, permeability can be predicted using FZI value and log porosity based on the following FZI equation;

$$\text{Permeability}(K) = \phi(FZI(1-\phi)/(0.0314\phi))^{\wedge 2} \quad (3)$$

Pore throat radius can be predicted from log porosity and modeled permeability using Winland equation. Finally, pore throat radius can be converted to capillary pressure by the following capillary equation;

$$Pc = 2\sigma \cos\theta/\text{radius} \quad (4)$$

This prediction method of permeability and capillary pressure will be re-evaluated and optimized in the next phase.

5. Geological Layering and Mapping

Results from geological framework modeling and rock type optimization were integrated in this part

5.1 Geological Layering

Time equivalent correlation was conducted for a realistic flow unit distribution by defining parasequence boundaries on slabbed cores. One parasequence is called in this study as geological layer, which has usually 2 or 3 reservoir layers defined by different petrophysical characteristics. One reservoir layer can be one flow unit. During cored well correlation, a useful relationship between lithofacies and porosity/micro-resistivity logs was found. Reworked and coarse-grained lithofacies at the base of parasequence in Lower IIB-IID is correlated to a high micro-resistivity and less porosity part. This will be used for uncored well correlation in the next phase. Finally, 40 geological layers were correlated among 44 cored wells (Fig.11).

5.2 Lithofacies and Permeability Mapping

Fig.24 shows lithofacies map for geological layer IID4. The defined lithofacies at 44 cored wells using slabbed cores and thin sections for this layer were interpolated using a geological template of palaeo-topographic interpretation map (Fig.13) on the aggradational lithofacies stacking concept (Fig.12).

Permeability map for this geological layer (Fig.25) was preliminarily produced using lithofacies map (Fig.24), log porosity and FZI regression values for each lithofacies. Although the obtained permeability map shows a fair match with actual core permeability, further optimization of FZI value for each rock type is planned in the next phase to accomplish even better match among predicted permeability, core permeability and dynamic data.

6. Discussion

Enormous geological information in terms of carbonate depositional style was derived mainly from polished slabbed cores. The most significant geological feature is abrupt lateral change and aggradational stacking of lithofacies particularly observed in Lower IIB-IID. Such geological feature rather matches with detached rimmed carbonate shelf model than carbonate ramp model, although a steep slope has not been observed in this reservoir. C.H.Moore[9] indicated that carbonate ramp and rimmed carbonate shelf are established in response to high-rate and slow relative sea-level rising conditions, respectively. This explanation seems to be suitable to explain the observed lithofacies distribution. In IIE-IIF, deep outer shelf depositional environment could have remained in a broad area, while sea-level fall is indicated by geological features such as dominant broken and algal affected orbitolina. In Lower IIB-IID, slow relative sea-level rising condition was interpreted based on the various geological features (Fig.10). A depositional style similar to detached carbonate rimmed shelf could have formed under this condition, overlapping on the emerged NW-SE trending shoal and tidal channel system after relative sea-level fall. Subtle progradational lithofacies stacking and unclear lateral lithofacies change in IIA-Upper IIB could be explained by a change in depositional style from detached rimmed shelf to carbonate ramp in response to the increased rate of relative sea-level rise.

A major question remains against this interpretation. Upward shallowing is the conventional understanding for the whole Thamama II sequence and is the base of progradational carbonate ramp model under highstand condition. This understanding depends on the presence of abundant rudist shell fragments and abundant small foraminifera such as milioliids and textulariids in IIA-Upper IIB and in the upper most part of IIA, respectively. The former might be explained by a change in development condition for rudists from an unoxic water during 3rd order global lowstand in Lower IIB-IID to an oxic water due to recovered oceanic circulation during 3rd order global transgression in IIA-Upper IIB. The latter seems to be over-impressed by less algal micritization on foraminifera grains in the uppermost part of IIA. Lots of micritized grains suspecting their foraminifera origin are observed particularly in Lower IIB-IID.

Preferential high permeability distribution in IIA-Upper IIB accords with the observed more non-micritized grains and intergranular pores in this interval than in the underlying subzones. This could be attributed to less algal micritization on bioclasts possibly due to a deeper water depth or continuous deposition with less frequent agitation of sediments under high-rate relative sea-level rising condition. High growth rate of carbonate producing organism such as rudist, and consequent rapid carbonate accumulation are also presumed in an oxic water environment.

After an integrated work between geological framework modeling and rock type optimization, lithofacies is regrouped into 'rock type' using FZI values. Lithofacies in this study is in accord with FZI concept, since lithofacies is classified based on grain types, which control physical property and micro-porosity distribution of grains, in close connection with pore shape/tortuosity as variables of FZI equation. Pore throat size analysis indicates that most of data show unimodal curve shape and these peak pore throat sizes can be estimated with Winland equation. Pore throat size is directly related with capillary pressure (Cp), independent of pore shape/tortuosity. Therefore, vital geological distribution information will be disintegrated if pore throat size or Cp is used as a key for rock typing. In stead, rock types defined by FZI allow their lateral/vertical distribution modeling in line with geological framework. Pore throat size or Cp is straightforwardly calculated with Winland equation if rock type has a unimodal curve shape.

Further optimization will be required for rock types with heterogeneous lithofacies, which has bimodal curve shape and relatively poor FZI regression.

7. Conclusion

- Adequate grain type identification using polished slabbed cores is a key for both geological framework modeling and rock type optimization in Thamama II carbonate reservoir, which has a complex petrographical and petrophysical relationship.

- NW-SE palaeo-topographic trend of a shoal and tidal channel system and 4th and 5th order relative sea-level change were found as major geological factors controlling distribution of permeability as well as lithofacies.

- Distribution of the defined 10 lithofacies based on the composition of newly defined 8 grain types shows an aggradational stacking pattern in Lower IIB-IID, matching with detached rimmed carbonate shelf model rather than carbonate ramp model. This depositional style could be attributed to the interpreted slow relative sea-level rising condition in this interval.

- Each of 13 (sub)lithofacies and 6 rock types was defined by one FZI value based on the agreement of such lithofacies/rock type, which has distinct grain type and pore type composition, with FZI concept.

- Lithofacies map was produced using core description and a geological template of palaeo-topographic map. Permeability map was generated using lithofacies map, log porosity and FZI poro-perm regression value for each rock type.

Acknowledgment

The authors would like to thank the management of ADNOC, JODCO and ZADCO for permission to publish this paper.

Reference

1. Purser, B.H. : "Sedimentation around Bathymetric Highs in the Southern Persian Gulf." In : Purser, B.H.(eds.) "The Persian Gulf." Springer-Verlag, 157-177, (1973)

2. Koepnick, R.B., Waite, L.E., Kompanik, G.S., Al-Shammery, M.J. and Al-Amoudi, M.O. : "Sequence Stratal Geometries and Burial-Related Microporosity Development: Control on Performance of the Hadriya Reservoir (Upper Jurassic) Berri Field, Saudi Arabia." GEO'94 Proceeding Vol.II, 615-623, (1994)

3. Vahrenkamp, V.C. : "Carbone Isotope Stratigraphy of the Upper Kharaib and Shuaiba Formations : Implications for the Early Cretaceous Evolution of the Arabian Gulf Region." AAPG Bulletin, V.80, No.5, (1996)

4. Burgess, C.J. and Peter, C.K. : "Formation, Distribution and Prediction of Stylolites as Permeability Barriers in the Thamama Group, Abu Dhabi." SPE13698, (1985)

5. Kolodzie Jr, S. : "Analysis of Pore Throat Size and Use of the Waxman-Smits Equation to Determine OOIP in Spindle Field, Colorado." SPE9382, (1980)

6. Martin, A.J., Solomon, S.T. and Hartmann, D.J. : "Characterization of Petrophysical Flow Units in Carbonate Reservoirs." AAPG Bulletin, V.81, No.5, (1997)

7. Amaefule, J.O. et al.: "Enhanced Reservoir Description : Using Core and Log Data to Identify Hydraulic (Flow) Units and Predict Permeability in Uncored Interval/Wells." SPE26436, (1993)

8. Lucia, F.J. : "Rock-Fabric/Petrophysical Classification of Carbonate Pore Space for Reservoir Characterization." AAPG Bulletin, V.79, No.9, (1995)

9. Moore, C.H. : "The Nature of Carbonate Depositional System." In : "Carbonate Diagenesis and Porosity." Development in Sedimentology 46, Elsevier, 1-18, (1989)

Fig.1 : Rock Type Models with Different Petrophysical Variation in Rock Types and Their Distribution

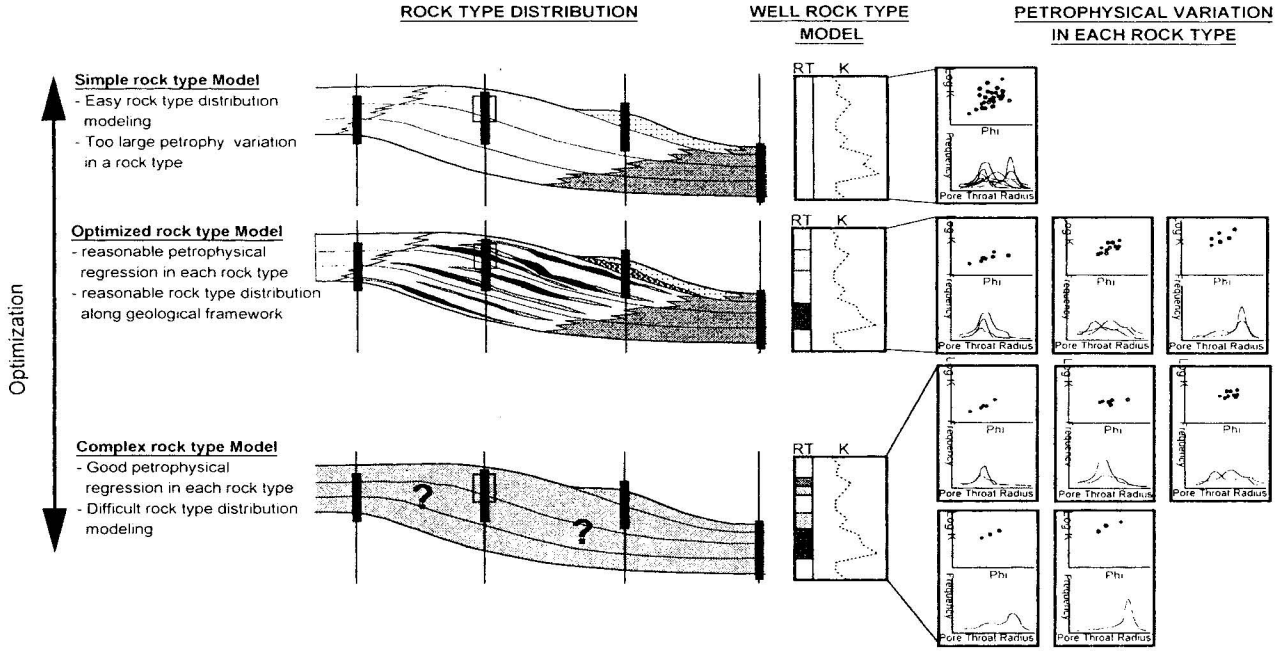

Fig.2 : Information Retained within Three Reservoir Rock Classification Categories

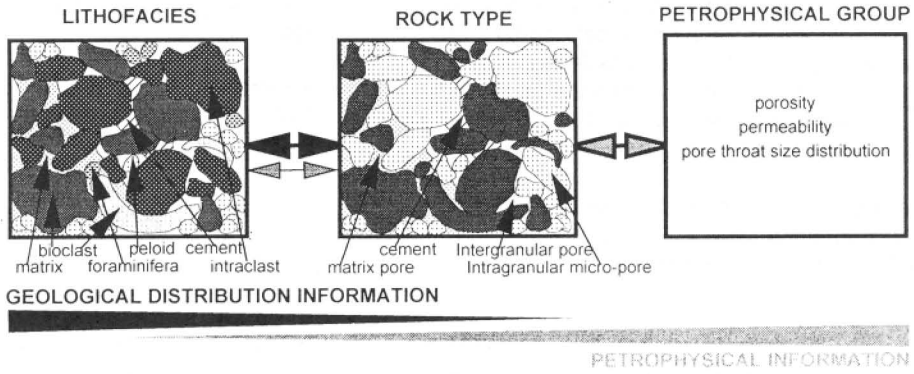

Fig.3 : Work Flow Chart for Thamama II Reservoir Characterization Study

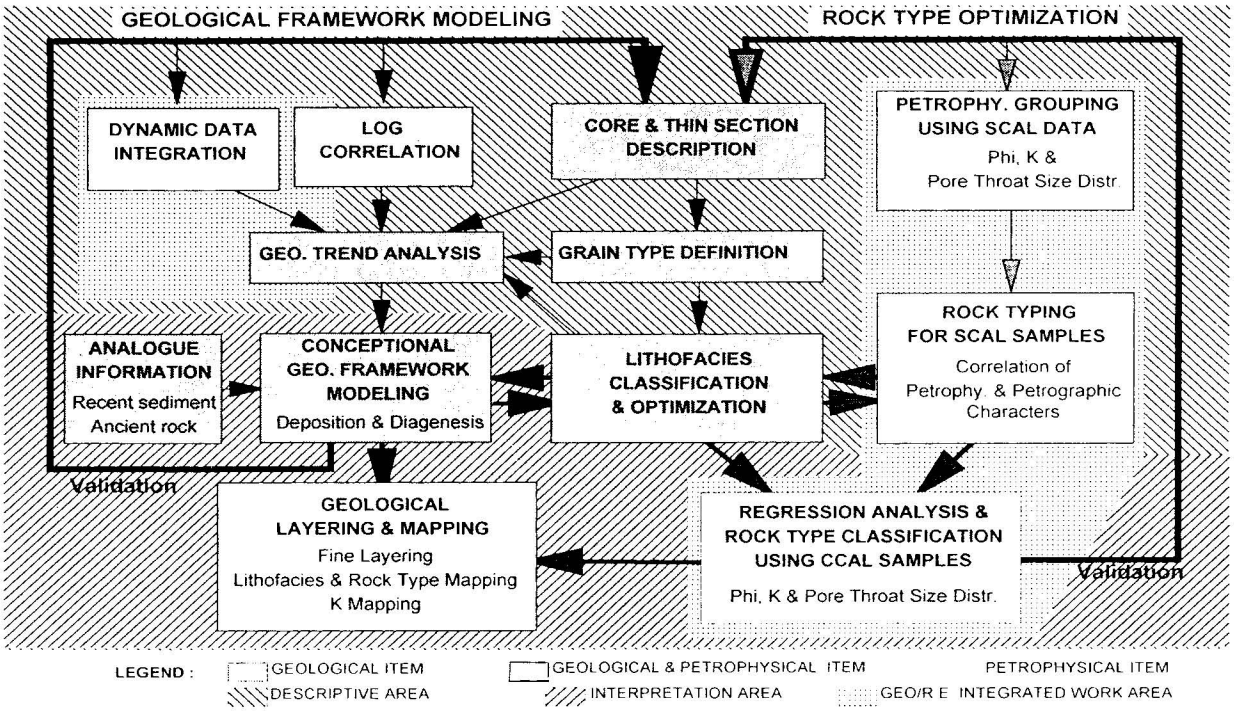

Fig.4 : Matrix Texture Plot for Thamama II SCAL Samples

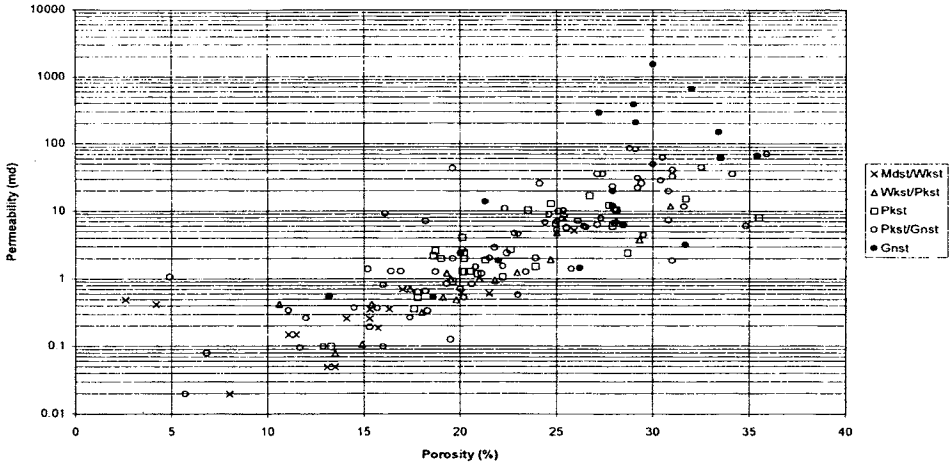

Fig.5 : Intergranular Porosity Occurrence Plot for Thamama II SCAL Samples

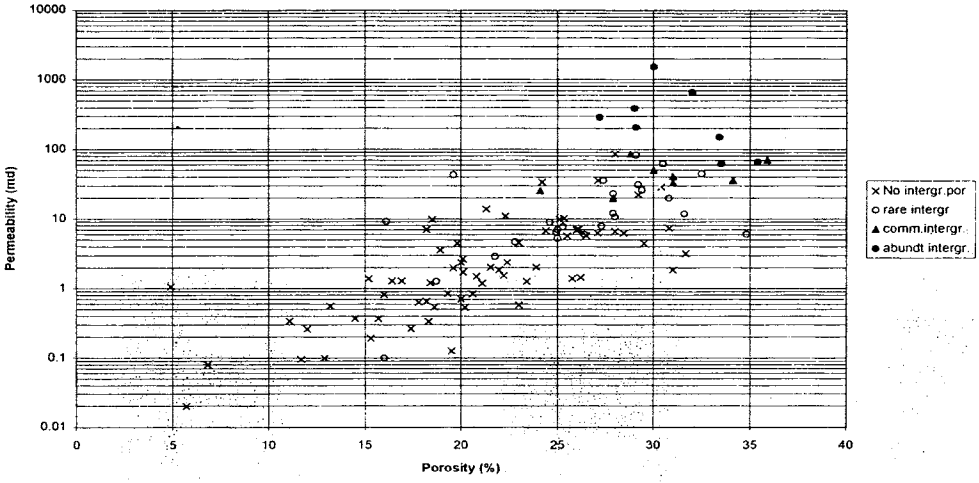

Fig.6 : Grain Type Identification by Thin Section and Slabbed Core

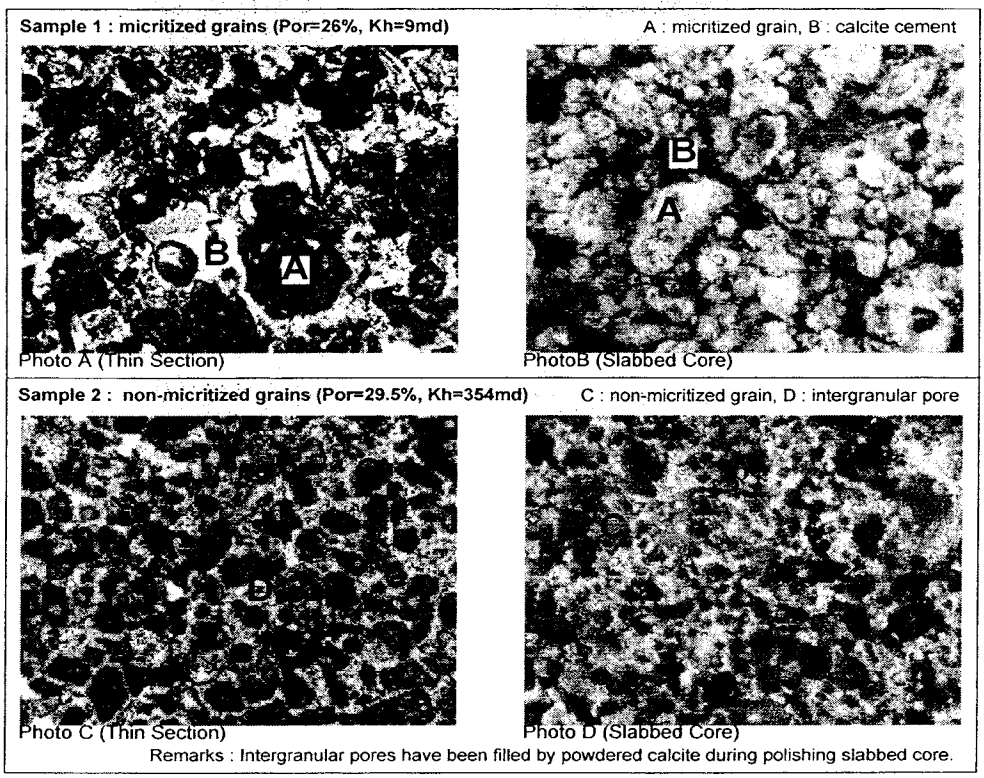

Fig.7 : Depositional Environment and Physical Property of Identified Coarse Grain Types

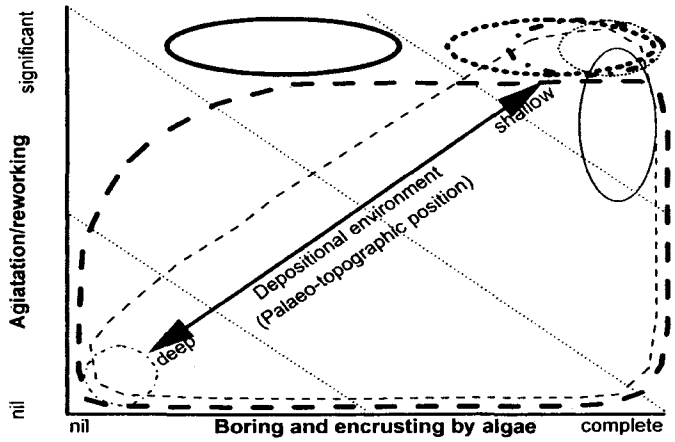

Grain type	Physical property	Micropores within grain
Intact and non-micritized rudist	hard	nil
Shell fragment	hard-soft	nil-abundant
Orbitolina	mod-soft	common-abdt
Altered-bioclast	hard	nil
Micritic wkst intraclast	soft	abundant
Algal bdst/*lithocodium* intraclast	mod-soft	common-abdt
Algal grain	mod	common common-abdt
Peloidal grst intraclast	mod-soft	

Fig.8 : Schemetic Depositional Model of Coarse Grain Types and Relating Lithofacies

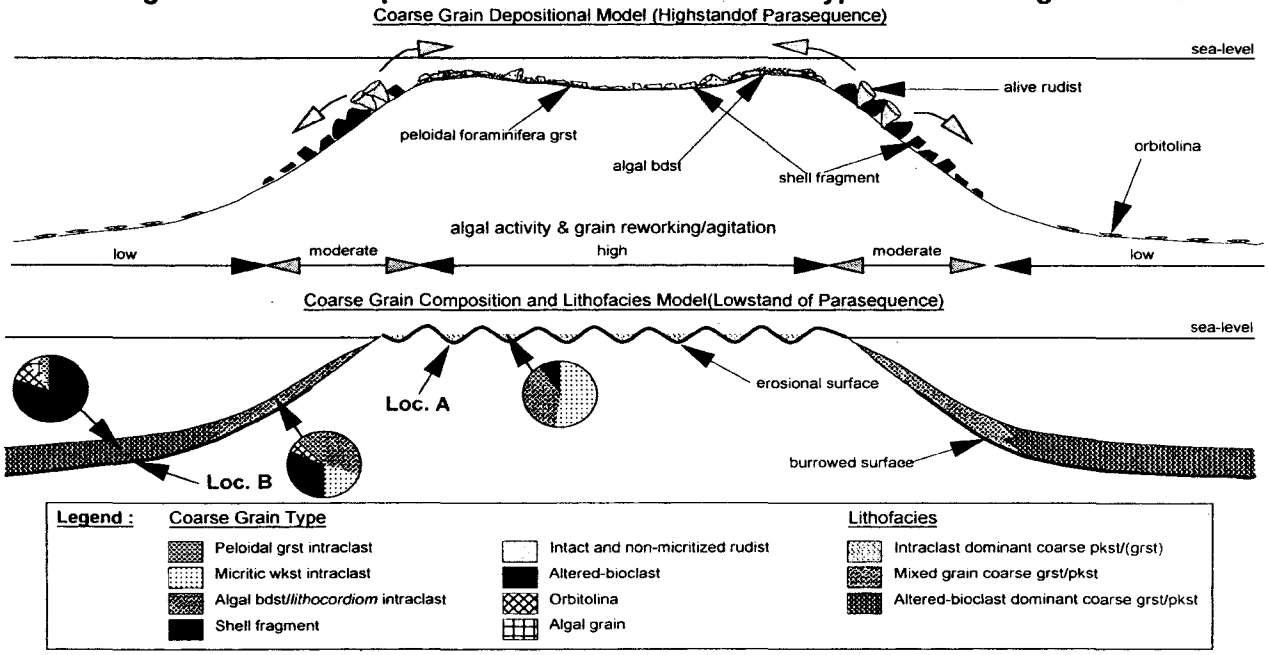

Fig.9 : Geological Features associated with Reworked Coarse Lithofacies

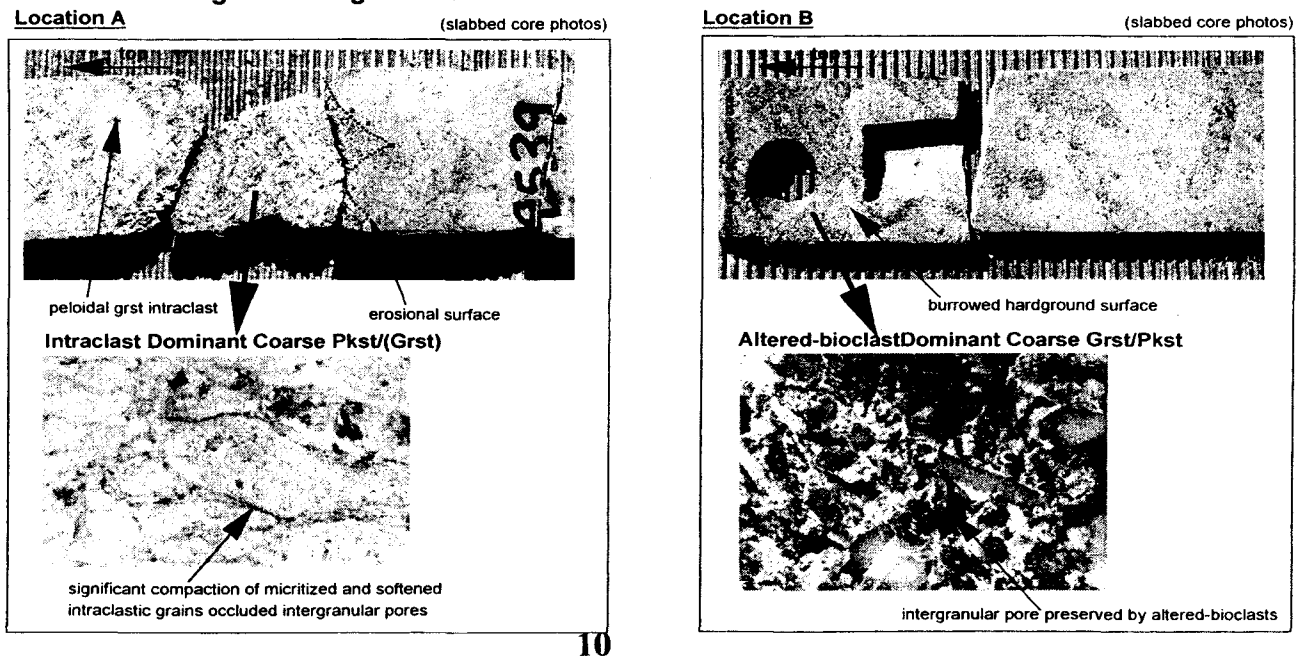

Fig.10 : Relative Sea-level Change Interpretation and Global Eustatic Correlation

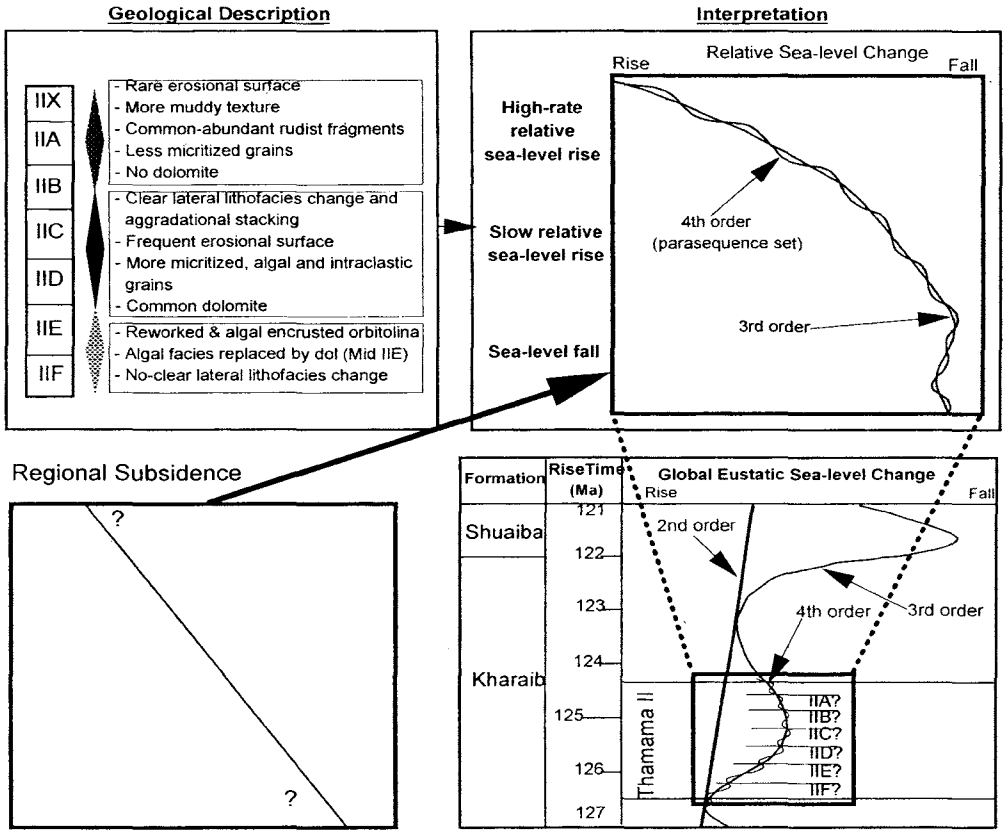

Fig.12 : Schematic Depositional Model for A Parasequence in 3 Intervals

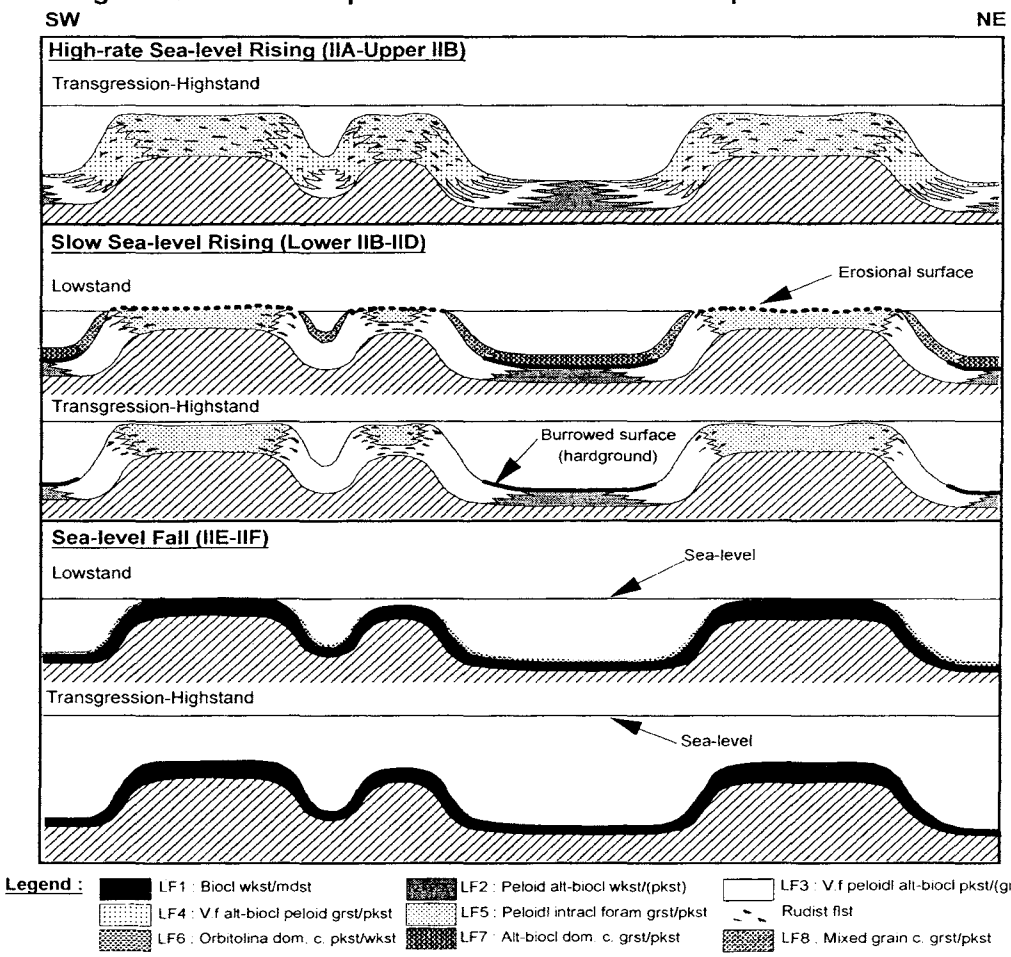

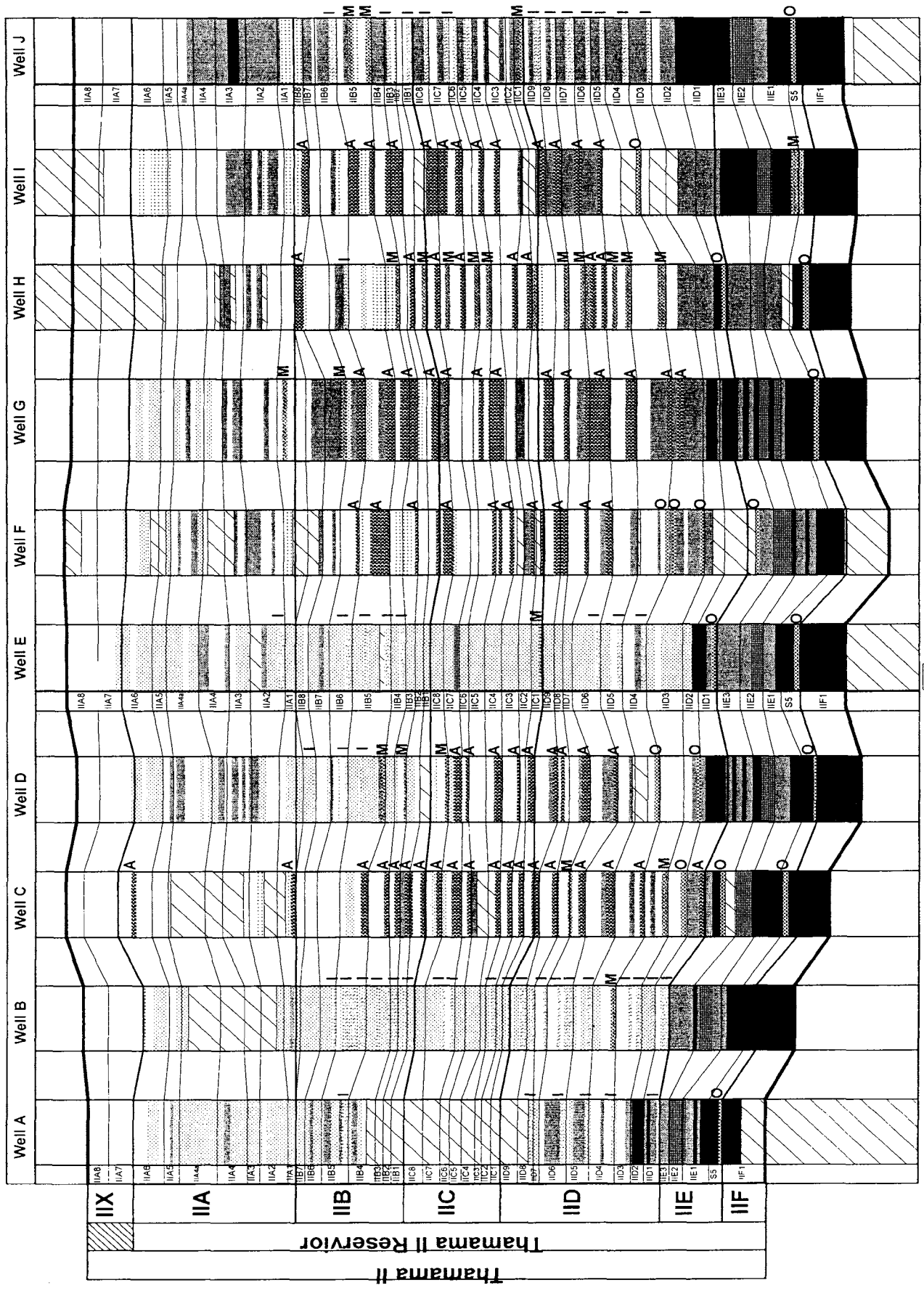

Fig.11 : NW - SE Stratigraphic correlation of Geological Layers in Thamama II

Fig.13 : Schematic Lithofacies Distribution Model (Thamama IID-Lower IIB)

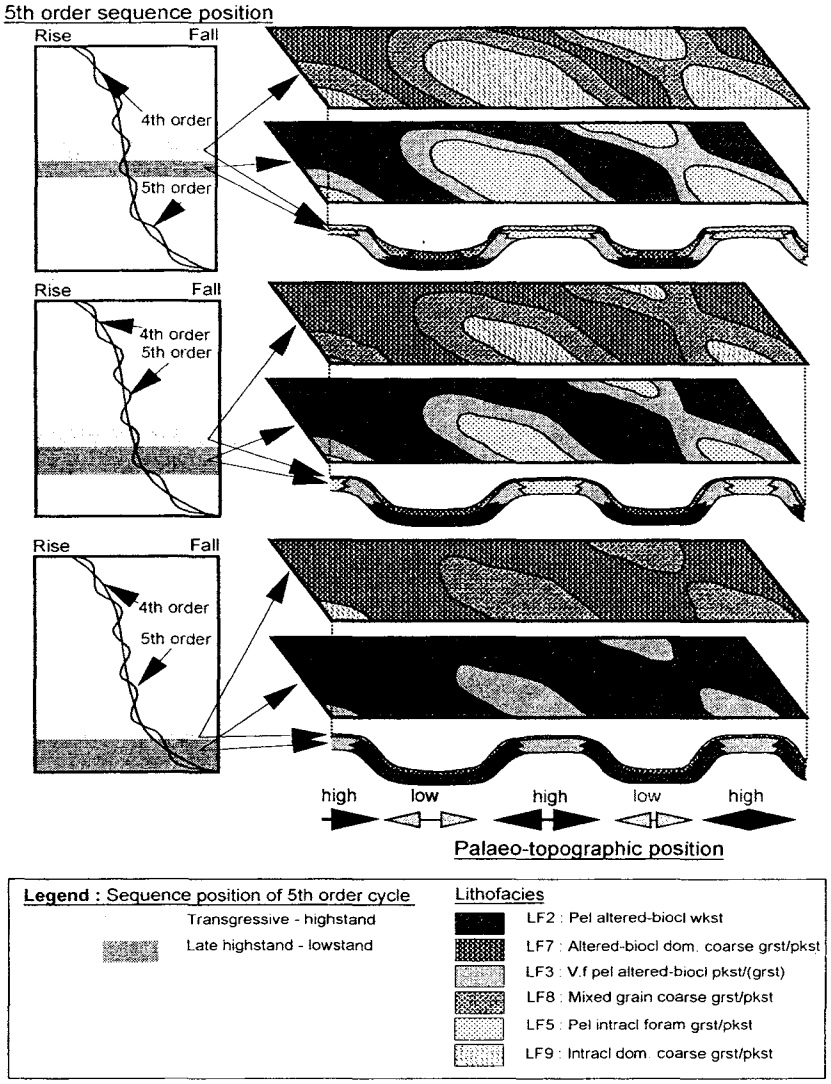

Fig.14 : Palaeo-topographic Interpretation Based on IID+IIE Isopach and Dolomite Distribution

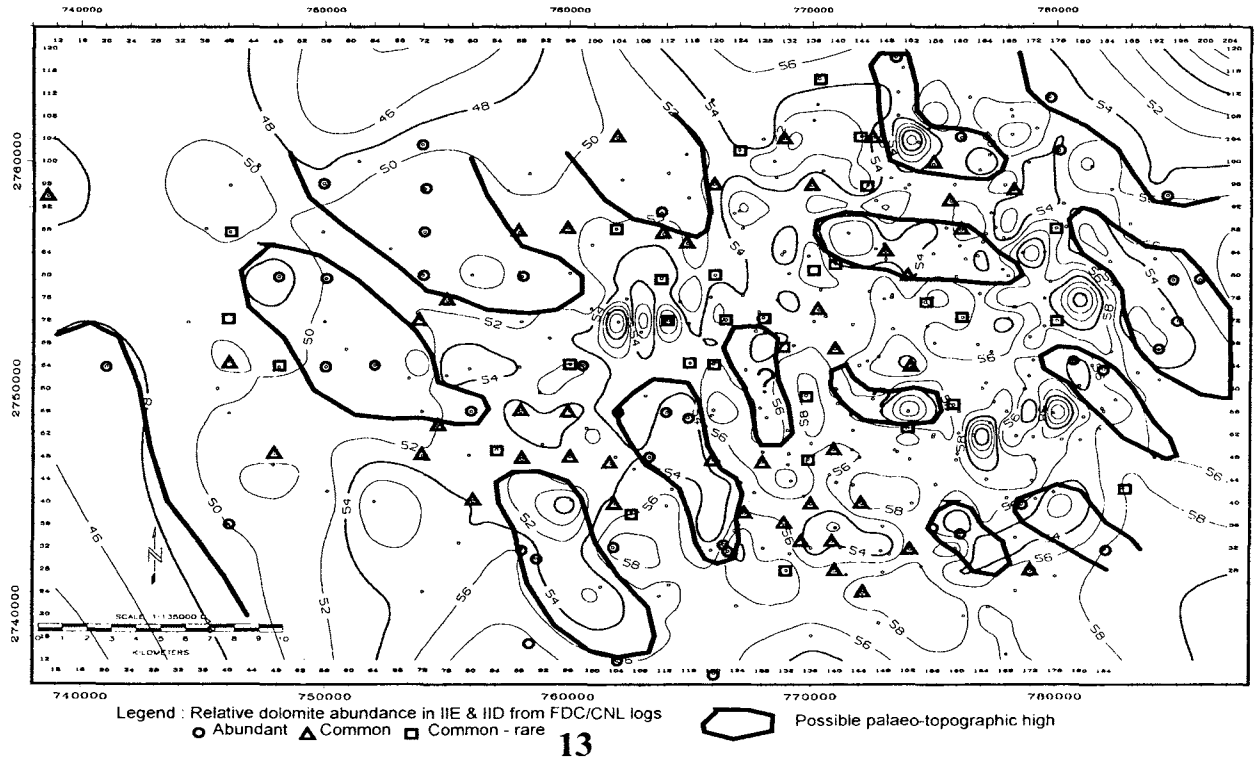

Fig.15 : Pore Throat Size Distribution Curve Types in Thamama II

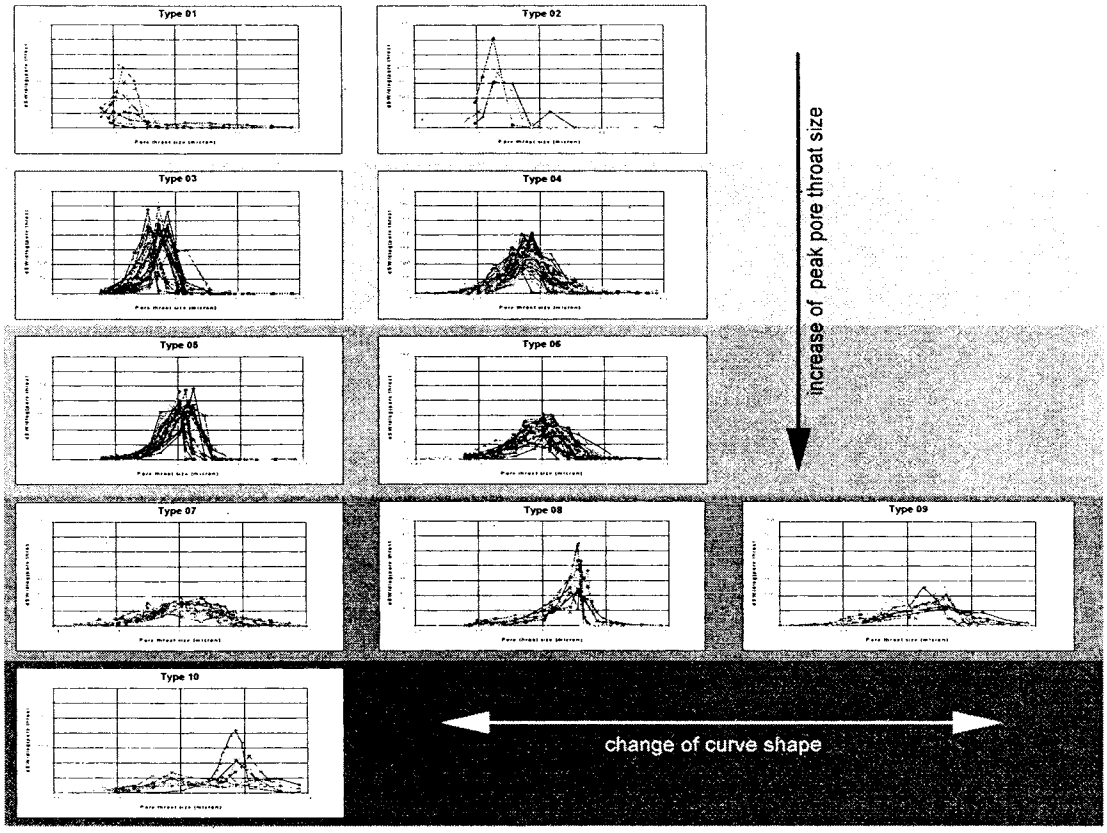

Fig.16 : Porosity vs. Permeability Plot with Pore Throat Size Distribution Curve Types

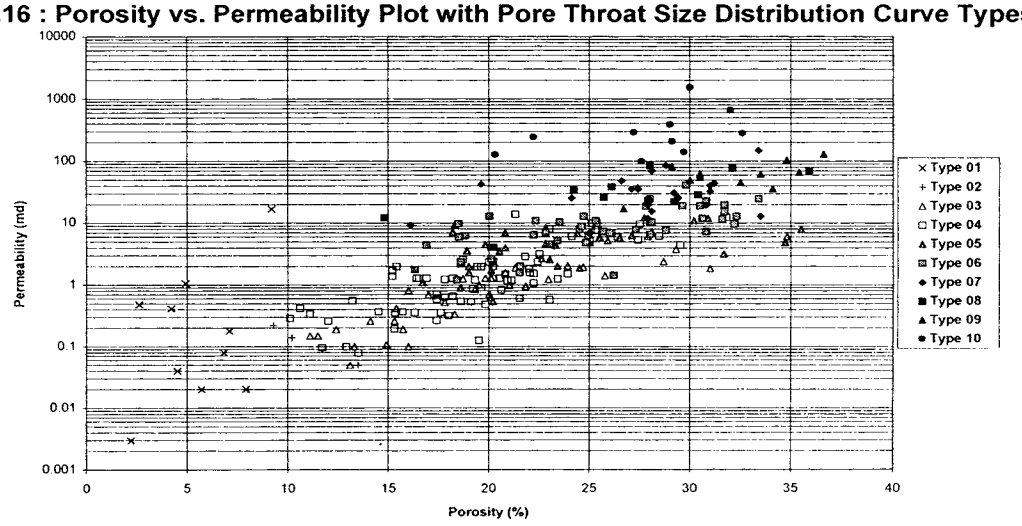

Fig.17 : Calculated Pore Throat Size from Winland Equation(R35)

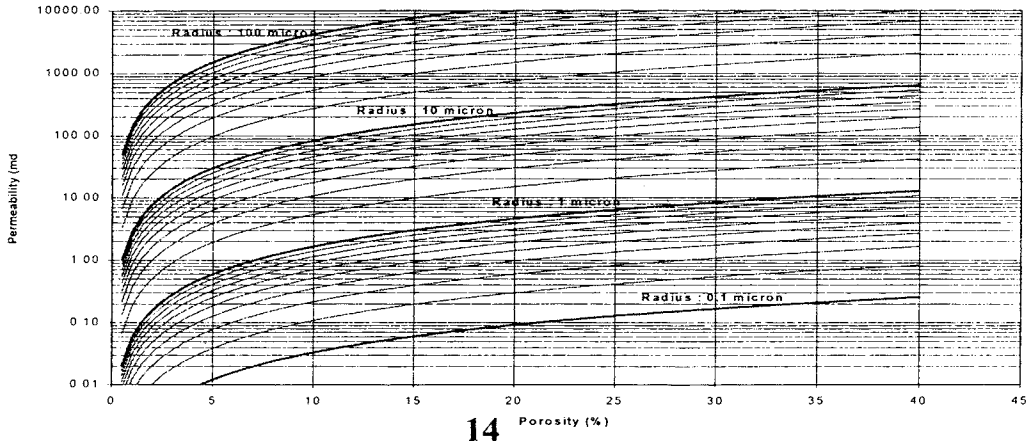

Fig.18 :Pore Throat Size Distribution Curve Plot for 10 Lithofacies

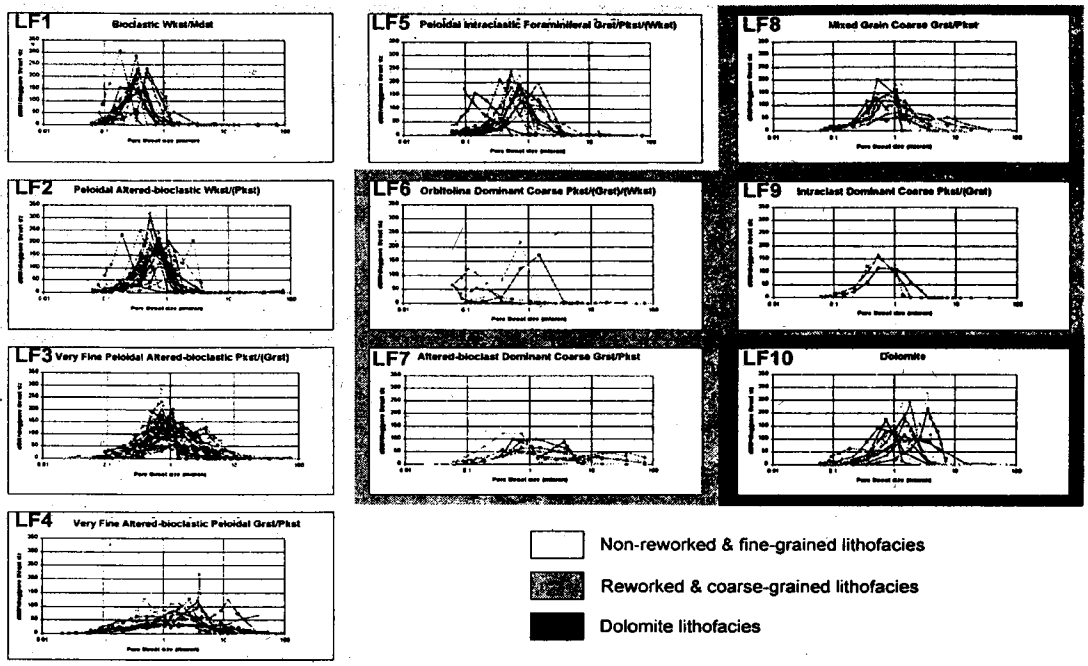

Fig.19 :Poro-perm Regression Analysis for LF3

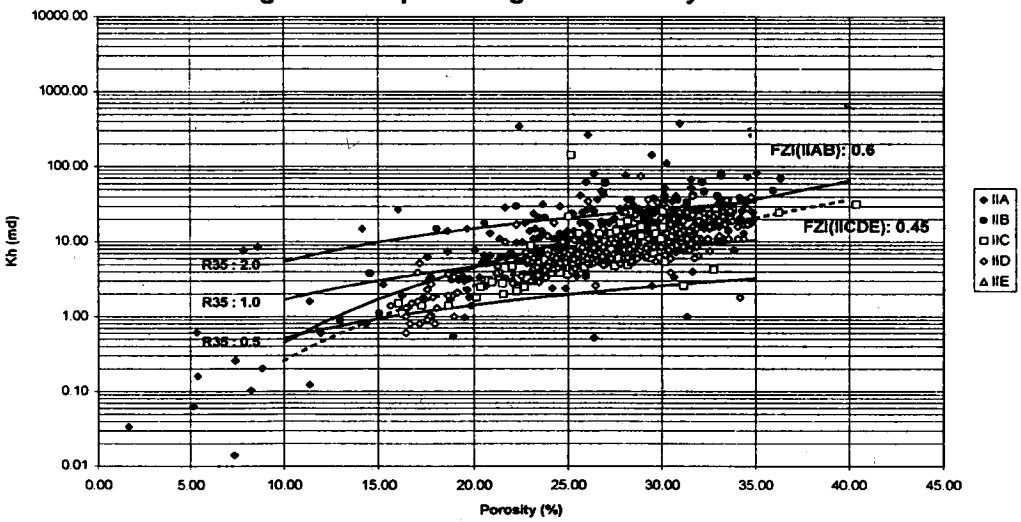

Fig.20 :Poro-perm Regression Analysis for LF5

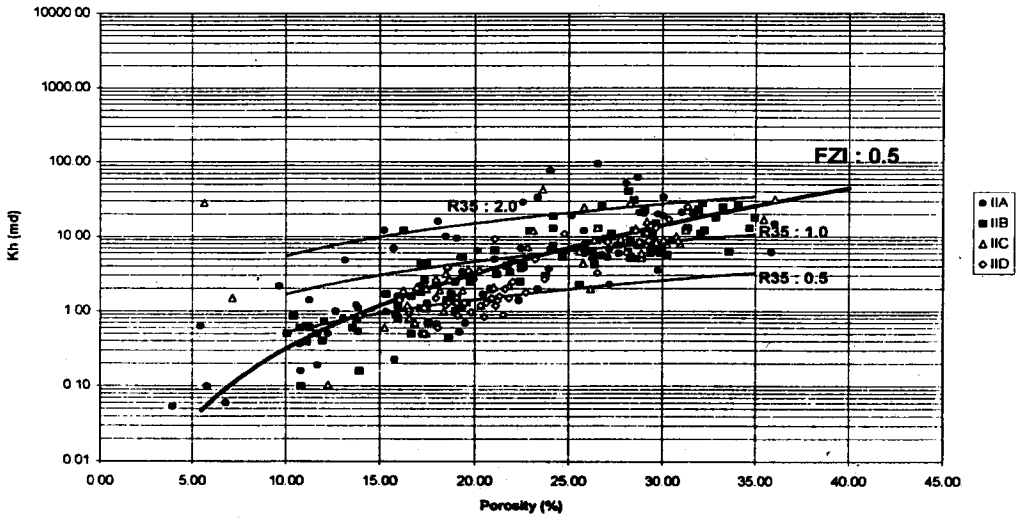

Fig.21 :Poro-perm Regression Analysis for LF7

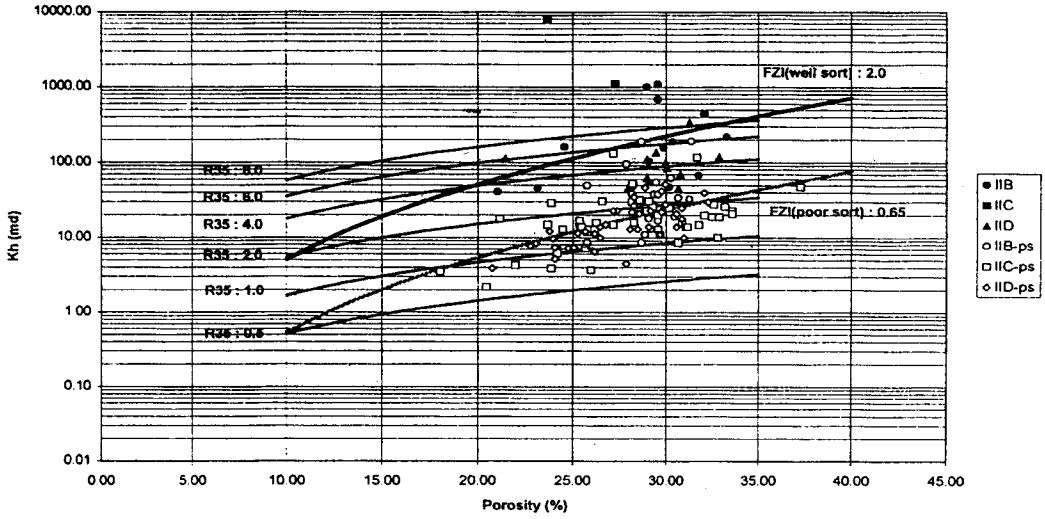

Fig.23 : Petrophysical Characters of 6 Rock Types

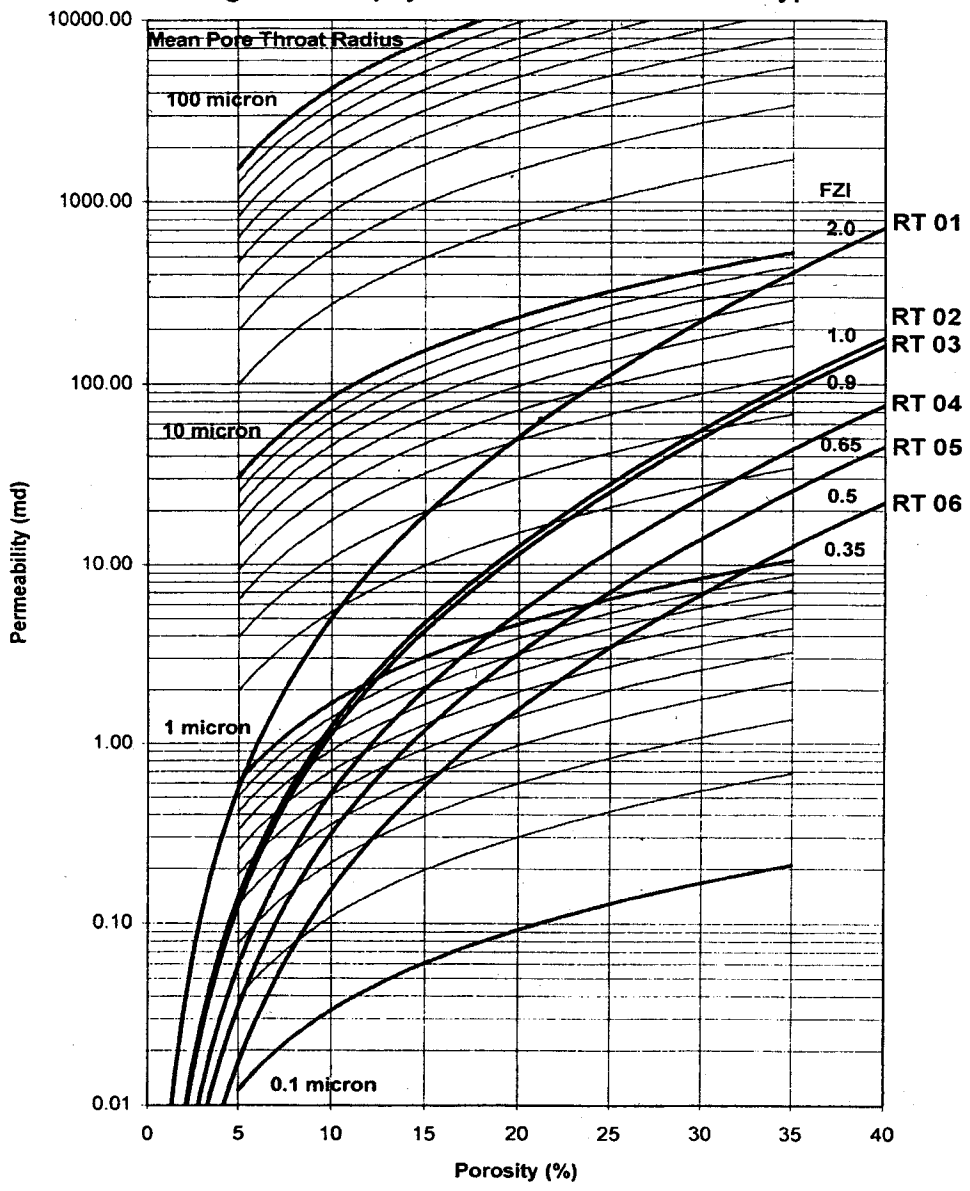

Fig.22 : Schematic Pore Type Composition of Lithofacies and Rock Types

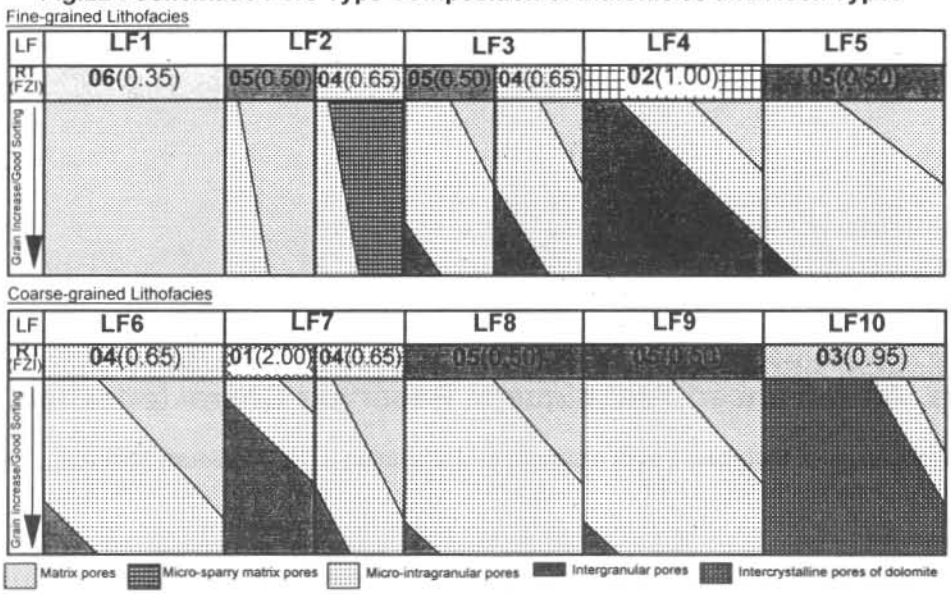

Fig.24 : Lithofacies Map for Geological Layer IID4

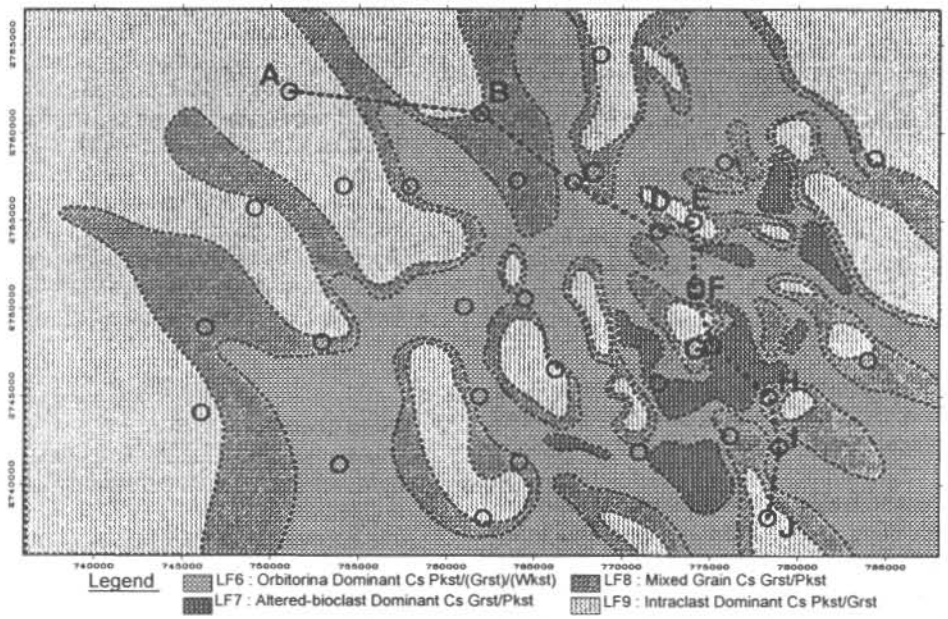

Fig.25 : Modeled Permeability Map for Geological Layer IID4